Available online at www.sciencedirect.com

SciVerse ScienceDirect

journal homepage: www.elsevier.com/locate/he

Spectroscopic characterization of Mn–Co–Ce mixed oxides, active catalysts for COPROX reaction

*Leticia E. Gómez, Eduardo E. Miró, Alicia V. Boix**

Instituto de Investigaciones en Catálisis y Petroquímica, INCAPE (FIQ UNL-CONICET), Santiago del Estero 2829, 3000 Santa Fe, Argentina

ARTICLE INFO

Article history:
Received 11 December 2012
Received in revised form
25 February 2013
Accepted 1 March 2013
Available online 29 March 2013

Keywords:
Mn–Co–Ce mixed oxides
COPROX
XPS
Raman
CO_2 tolerance
Hydrogen

ABSTRACT

Mn–Co–Ce mixed oxides are active and selective catalysts for the CO preferential oxidation (COPROX), which is a promising process for the purification of hydrogen streams. In this work, we report a careful spectroscopic characterization of the said system, with the aim of relating its physical chemistry properties to the catalytic behavior. In all the Co–Mn–Ce samples, we detected the formation of partially developed $(Mn,Co)_3O_4$ mixed spinels. The presence of these species, which can be reduced during the TPR experiments at an intermediate temperature range (300–600 °C), was also suggested by XRD and LRS. XPS results show that in all cases the catalytic surface is enriched in Mn, while the opposite occurs for Co. As regards the catalytic activity, we observed that the best formulations were those containing intermediate Mn/Co ratios (1/4 and 1/1), which can be ascribed to the promoting effect of Mn in improving the redox properties of Co active sites and provoking an increase in surface area. The best catalyst, which has a Mn/Co ratio of 1/4, was very stable after 75 h of time-on-stream with CO_2 included in the feed.

1. Introduction

The hydrogen used as a fuel in the PEMFC system is commonly generated from the reforming of alcohols or hydrocarbons. Generally, that step is followed by the water gas shift reaction, where the hydrogen production is increased and the CO content of this effluent varies between 0.5 and 2%. Before entering the cell, the CO concentration in the hydrogen-rich stream must be less than 10 ppm in order not to deteriorate the cell anode. Several methods have been used to purify hydrogen; among these alternatives the CO preferential oxidation with O_2 is an effective option [1–4].

With the aim to eliminate CO in the hydrogen-rich stream without consuming H_2, several authors have developed successful catalysts based on precious or noble metals, achieving excellent results [5–12], but the elevated cost of these materials have led researchers to investigate other alternatives based on low-cost materials.

Numerous articles on transition metal-ceria systems have been published, in which CeO_2 plays a fundamental role in redox reactions due to its facility to release and storage oxygen. Likewise, the $CuO–CeO_2$ system has also been widely studied by several authors and the results obtained in COPROX are comparable to those reached by noble catalysts on a great number of occasions [13–16].

In a previous work, we studied the $CoO_x–CeO_2$ system prepared by the co-precipitation method and very successful results were obtained [17]. It was found that CeO_2 improved the re-oxidation of Co^{2+} to Co^{3+}, which is the active species for COPROX. Numerous publications showed that the addition of other metals to a cerium-based mixed oxides increases the oxygen-storage capability of the ceria. This effect is originated

* *Corresponding author*. Tel.: +54 342 4536861.
E-mail address: aboix@fiq.unl.edu.ar (A.V. Boix).

0360-3199/$ – see front matter
http://dx.doi.org/10.1016/j.ijhydene.2013.03.004

by the increase of the surface-oxygen mobility due to chemical interactions between cerium and the other metals [18–21].

In this vein, Zhao and co-workers added Co_3O_4 to $Ce_xMn_{1-x}O_2$ composites and obtained very good results in the COPROX reaction [22]. Guo et al. also investigated Co–Mn–Ce mixed-oxide systems. These authors showed excellent values of CO conversion for a high-Co content catalyst [23,24]. The addition of Mn to Co_3O_4 was also analyzed by Zhang et al., who attained a remarkable improvement in the catalytic performance of the cobalt oxide [25].

In this work, we studied the addition of manganese to the CoO_x–CeO_2 system using a battery of characterization techniques. A series of catalysts containing Mn, Co and Ce were prepared by the simultaneous co-precipitation of Mn, Co and Ce nitrates, and several Mn/Co molar ratios were studied in order to get the most active catalyst and to gain insight into the nature of Mn–Co–Ce interactions.

A very detailed analysis of the species present in these complex systems was carried out, especially to investigate the influence of Mn on the catalyst performance. For this purpose, a thorough study of the species was performed by means of X-ray photoelectron spectroscopy (XPS) and Laser Raman spectroscopy (LRS). The presence of different phases in the catalysts was analyzed by X-ray diffraction (XRD), and the reducibility of the materials was studied by means of temperature-programmed reduction (TPR). Furthermore, the stability of the most active catalyst was evaluated for more than 75 h in the COPROX reaction and in the presence of CO_2.

2. Experimental

2.1. Preparation of catalysts

MnCoCe catalysts were synthesized by the co-precipitation method. Aqueous solutions of $Co(NO_3)_2{\cdot}6H_2O$, $Ce(NO_3)_3{\cdot}6H_2O$ and $Mn(NO_3)_2{\cdot}4H_2O$ were simultaneously added into a continuously stirred flask in adequate amounts to get 10 wt.% of Co and Mn/Co molar ratios of 1/8, 1/4, 1/1 and 4/1 in each catalyst. An aqueous solution of $NH_4(OH)$ was added dropwise to the flask and then, the mixture was kept 2 h under continuous stirring. The precipitate obtained was washed several times in deionized water, and then dried overnight at 110 °C. The resulting powders were calcined at 450 °C for 4 h under air flow. The catalysts were labeled as MnCoCe(1/8), MnCoCe(1/4), MnCoCe(1/1) and MnCoCe(4/1), the fractions between brackets being the molar ratio Mn/Co in each sample. CeO_2 and bi-component samples MnCo, MnCe were also prepared by the co-precipitation method using the same conditions and reactants. A previously prepared CoCe catalyst was also taken into account to be compared with the other samples [17].

2.2. Catalytic tests

Preferential CO oxidation experiments were performed in a fixed-bed flow reactor at atmospheric pressure. Powder samples were placed in a tubular quartz reactor (8 mm i.d.). The reaction mixture consisted of CO 1%, O_2 1% and H_2 40%, He balance. In some runs, water (10%) and CO_2 (20%) were also fed. The weight/total flow ratio was adjusted to 2.1 mg cm^{-3} min by means of mass flow controllers.

The CO conversion and the selectivity toward CO_2 were defined as:

$$C_{CO} = 100 \cdot \left(1 - [CO]/[CO]^{\circ}\right)$$

$$S = 100 \cdot [CO_2]/2 \cdot \left([O_2]^{\circ} - [O_2]\right)$$

where [CO], [CO_2] and [O_2] were reactor exit concentrations and [CO]°, [O_2]° represented feed concentrations, which were measured with a GC-2014 Shimadzu chromatograph equipped with a TCD cell. All the catalysts were pretreated during 30 min in a 10% O_2/He mixture at 200 °C before the catalytic test.

In order to study a possible deactivation caused by CO_2 as the one reported in [24], the MnCoCe(1/4) catalyst was analyzed in a stability COPROX test at 175 °C during 75 h, adding 20% CO_2 in the feed.

2.3. Catalysts characterization

2.3.1. Chemical composition determinations

Elemental analyzes were performed by inductively coupled plasma atomic emission spectroscopy (ICP-AES) on a ICP-OPTIMA 2100 DV Perkin Elmer instrument.

2.3.2. Textural properties

N_2 adsorption isotherms were obtained at −196 °C with a Micromeritics Gemini V instrument. The BET equation was used for calculating the specific surface area of the materials and the average pore size was calculated using a BJH formula from the desorption branch of the N_2 adsorption isotherm. Prior the measurement, the samples were degassed under vacuum at 300 °C overnight.

2.3.3. X-ray diffraction (XRD)

The patterns of all powder samples were measured on a Shimadzu XD-D1 instrument with monochromator using Cu-Kα radiation at a scanning rate of 1°min^{-1} in $2\theta = 20$–80°.

2.3.4. Laser Raman spectroscopy

The Raman spectra of calcined powders were recorded using a LabRam spectrometer (Horiba-Jobin-Yvon) coupled to an Olympus confocal microscope (a 100× objective lens was used for simultaneous illumination and collection), equipped with a CCD detector cooled to about 200 K using the Peltier effect. The excitation wavelength was in all cases 532 nm (SpectraPhysics diode pump solid state laser). The laser power was set at 30 mW.

2.3.5. Temperature-programmed reduction (H_2-TPR)

The reduction under hydrogen was measured in a Micromeritics 2920 instrument. The reducing gas was a 2% H_2/Ar mixture (25 ml min^{-1}), the temperature was ramped up at 10 °C min^{-1} to 900 °C. In all cases, a mass of 100 mg was placed in a quartz U-shaped reactor. Prior the TPR test, the samples were pretreated in Ar at 200 °C for 30 min in order to clean the surface.

2.3.6. X-ray photoelectron spectroscopy

XPS analyzes were performed in a multi-technique system (SPECS) equipped with a dual Mg/Al X-ray source and hemispherical PHOIBOS 150 analyzer operating in the fixed analyzer transmission (FAT) mode. The spectra were obtained with pass energy of 30 eV, the Al Kα X-ray source ($h\nu = 1486.6$ eV) was operated at 100 W. Also, the spectra of Ce 3d, O 1s and C 1s were measured with MgKα X-ray source ($h\nu = 1253.6$ eV) in order to avoid the interference of the Mn LMM region of Auger transitions with Ce 3d core-level. The working pressure in the analyzing chamber was less than 2.0×10^{-8} mbar. The XPS analyzes were performed on the calcined powders. The spectra regions corresponding to Co 2p, O 1s, Ce 3d, Mn 2p, Mn 3s and C 1s (reference 284.6 eV) core levels were recorded for each sample. The data treatment was performed with the Casa XPS program (Casa Software Ltda., UK). The peak areas were determined by integration employing a Shirley-type background. Peaks were considered to be a mixture of Gaussian and Lorentzian functions in a 70/30 ratio.

3. Results and discussion

The compositions of the samples analyzed by ICP are introduced in Table 1, and are in agreement with the predefined nominal values. The BET method was used to determine the specific area of each sample and the values are also reported in Table 1. As it can be observed, the specific surface of CeO_2 increases when a little amount of manganese is added to the structure. In the MnCoCe samples, as the Mn content increases, the surface area also increases until Mn/Co = 1/1. With a high content of Mn, in MnCoCe(4/1) the surface area decreases. For all samples, the average pore size increases with the manganese addition and corresponds to the mesoporous range.

3.1. Catalytic performance

Fig. 1 shows the CO conversion and selectivity of O_2 toward CO_2 for the preferential oxidation of CO over MnCoCe catalysts with different Mn/Co molar ratios. The CoCe and MnCe catalysts are also included for comparison. At low temperature (≤125 °C) the Mn addition, with (1/4) and (1/1) molar ratios, significantly improved the CO conversion compared with CoCe catalyst, where the selectivity was close to 100%.

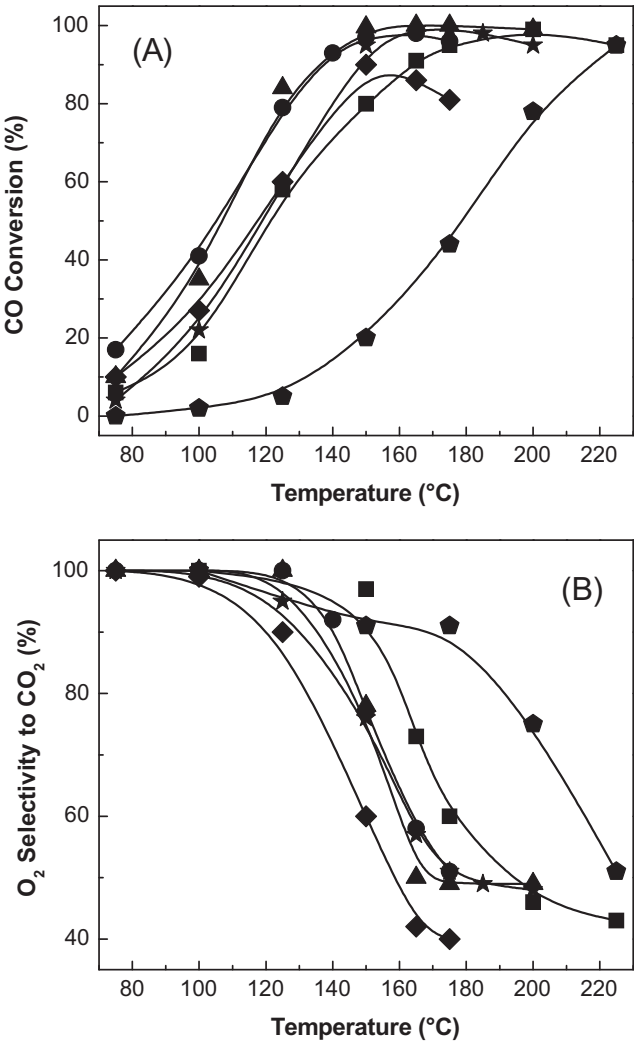

Fig. 1 – Catalytic performance of catalysts: ■MnCoCe(1/8), ▲MnCoCe(1/4), ●MnCoCe(1/1), ◆MnCoCe(4/1), ★CoCe, ⬟MnCe. (A) CO conversion, (B) Selectivity of O_2 to CO_2. Reaction conditions: 1% CO, 1% O_2, 40% H_2 in He balance. Catalyst weight/total flow: 2.1 mg cm^{-3} min.

Table 1 – Chemical composition and textural properties.

Samples[a]	Mn[b] (wt.%)	Co[b] (wt.%)	BET surface area ($m^2\ g^{-1}$)	Average pore diameter (Å)	Pore volume ($cm^3\ g^{-1}$)
CeO_2	–	–	93	52	0.13
MnCe	0.94	–	115	70	0.20
MnCo	14.6	66.1	87	81	0.19
CoCe	–	8.4	93	78	0.16
MnCoCe(1/8)	1.1	10.2	145	48	0.20
MnCoCe(1/4)	2.6	11.0	165	52	0.24
MnCoCe(1/1)	9.9	10.4	171	59	0.31
MnCoCe(4/1)	43.6	11.2	108	78	0.23

a The molar ratio Mn/Co between brackets.
b Composition measured by ICP-AES.

The most active catalyst, MnCoCe(1/4), reached 100% CO conversion at 150 °C and remained constant to 180 °C. The selectivity at 150 °C was 80% and then, it declined with the temperature increase.

The MnCoCe(1/1) catalyst, whose manganese and cobalt content are similar, also resulted very active with almost complete conversion at 150–175 °C. The selectivity curve was similar to that of sample MnCoCe(1/4), selectivity being 100% until 125 °C then decreasing with the increase of temperature. However, when the temperature was 140 °C the conversion and selectivity reached 93% and 91%, respectively. For the previously studied CoCeO catalyst, the conversion was almost 100% but at higher temperatures, between 165 and 185 °C, thus confirming the beneficial effect of the Mn promoter [17].

The MnCoCe(1/8) catalyst, with a lower content of manganese, was very active in a wide range of temperatures,

showing a CO conversion close to 95%, between 175 and 225 °C. The shape of the selectivity curve was similar to that of other catalysts, but in this case a slight increment was observed. At 150 °C, when the CO conversion is 80%, the selectivity is about 97% and then, the curve follows the same trend as previous catalysts.

The catalysts with higher manganese loading, MnCoCe(4/1), achieved its maximum conversion of 90% at 150 °C, and then it decreased as the temperature increased. Beyond the low conversion with respect to the previous catalyst, the selectivity also showed a pronounced decrease at lower temperature. The low activity of catalysts with high Mn loading could be related to the surface area decrease and the lack of accessibility of reactant molecules to Co active sites.

On the other hand, the sample without cobalt was the least active catalyst, conversion being 95% at 225 °C. In a similar way, selectivity showed a declining trend with increasing temperature.

In agreement with our results, for the same reaction, Zhao et al. [22] reported very good catalytic performance with 20 wt.% $Co_3O_4/Ce_{1-x}Mn_xO_2$ catalysts prepared by the SACP method. The complete CO conversion was reached in a wide temperature range (130–200 °C).

The effect of CO_2 addition in the feed on the catalytic behavior and stability of the most active catalyst was studied. For this purpose, the MnCoCe(1/4) catalyst was analyzed in the COPROX reaction at 175 °C, adding 20% CO_2 to the feed. Fig. 2 shows that after 75 h of time-on-stream, the catalyst maintained 95% of CO conversion while the selectivity slightly increased from 50 to 60%. At the end of this experiment, an LRS spectrum was performed, in which carbon formation was not observed. However, when H_2O (10%) was also fed, the CO conversion decreased to 51%.

In this vein, Guo et al. showed the complete CO conversion between 80 and 180 °C over Mn–Co–Ce catalysts with a higher cobalt content than our catalysts. However, this catalyst suffered a deactivation before 24 h of reaction, when the CO_2 was in the feed. The authors attributed this deactivation to the formation of carbonate species [23,24].

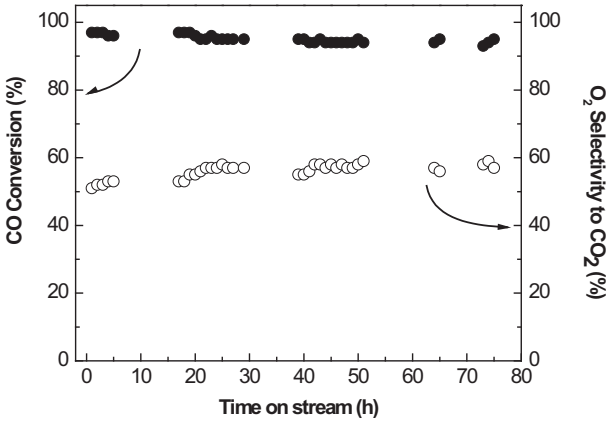

Fig. 2 – Long term stability test for COPROX on the MnCoCe(1/4) catalyst at 175 °C. Reaction conditions: 1% CO, 1% O_2, 20% CO_2, 40% H_2 in He balance. Catalyst weight/total flow: 2.1 mg cm^{-3} min.

3.2. *Catalysts characterization*

Fig. 3 shows the diffraction patterns of pure ceria, CoCe, MnCe, MnCo and MnCoCe catalysts synthesized by the co-precipitation method.

The CoCe diffractogram shows the most important peaks corresponding to CeO_2 (2θ = 28.6, 33.4, 47.8 and 56.6°) and Co_3O_4 (2θ = 31.3, 36.8, 44.8, 59.4 and 65.3°) phases (JCPDS 34-0394 and JCPDS 42-1467 respectively). In the MnCe sample, only the CeO_2 pattern appears and no signals of manganese oxides are observed, possibly due to their low concentration. In a similar way, the MnCo sample only shows the diffraction peaks associated with Co_3O_4.

The diffraction patterns of MnCoCe catalysts show different phases depending on the relative concentration of elements present. In the MnCoCe(1/8) catalyst, a broadening of peaks corresponding to the CeO_2 phase was observed. These results could indicate that the structure of CeO_2 is distorted due to the insertion of manganese, although the type-fluorite structure of CeO_2 is still maintained [26]. Also, in the main signal of CeO_2 (2θ = 28.6°), there appears an asymmetric broadening associated with an incipient formation of the $(Mn,Co)_3O_4$ phase, which has a characteristic peak at 29.4° (PDF 18-408). Likewise, the main peak of the $(Mn,Co)_3O_4$ phase (2θ = 36.4°) appears in this sample at 36.9°, close to the main signal of the Co_3O_4 spinel. The MnCoCe(1/4) pattern shows a similar behavior.

In MnCoCe(1/1), the peaks at 28.7° and 36.7° might belong to an incipient formation of the mixed spinel $(Mn,Co)_3O_4$. As the Mn content increases, the peak at 28.6° shifts to 28.7° for MnCoCe(1/4) and (1/1). However, the peak broadening could be due to lower degree of crystallinity or smaller particle size.

Finally, in sample MnCoCe(4/1), where a large content of manganese is incorporated, the mixed spinel $(Mn,Co)_3O_4$ is well developed. The characteristic signals of Bragg angles at

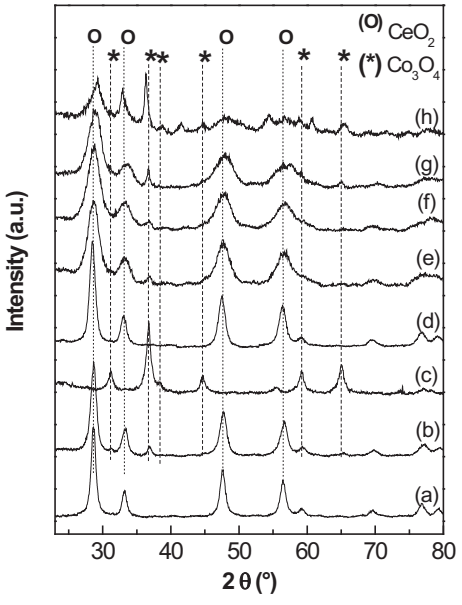

Fig. 3 – XRD patterns: (a) CeO_2, (b) CoCe, (c) MnCo, (d) MnCe, (e) MnCoCe(1/8), (f) MnCoCe(1/4), (g) MnCoCe(1/1) and (h) MnCoCe(4/1).

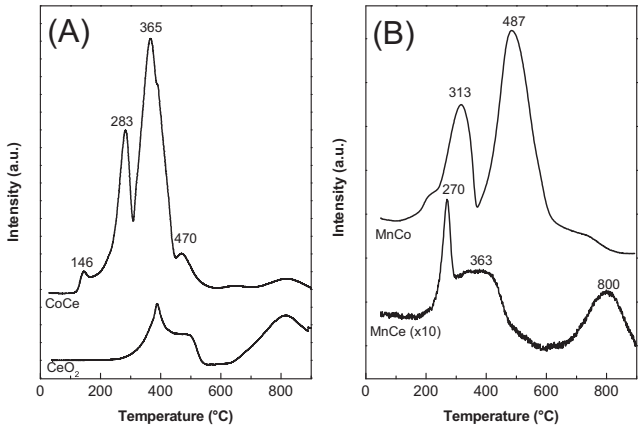

Fig. 4 – Temperature-programmed reduction. (A) CeO_2 and CoCe samples. (B) MnCe and MnCo samples.

29.3°, 32.9°, 36.3°, 44.6° confirm the presence of this phase. Mn_3O_4 and Co_3O_4 phases could also be present.

Similar formulations of the CoMnCe system prepared with different proportions of the constituent elements have shown the coexistence of two phases, Co_3O_4 and CeO_2 [22,23]. On the other hand, many other studies demonstrated the formation of the $Mn_xCo_{3-x}O_4$ solid solution in the Mn–Co–O binary oxide prepared by different methods [25,27].

Fig. 4A shows the reduction profiles (TPR) of the CoCe catalyst and pure CeO_2. It is known that the cobalt-oxide reduction could occur in two steps: Co^{3+} to Co^{2+}, between 200 and 300 °C with a maximum at 283 °C and Co^{2+} to Co^0 at a slightly higher temperature [28]. A small peak at 146 °C could also be observed, which was assigned to cobalt species highly dispersed on the ceria surface [22]. The ceria profile presents small peaks centered at 365 and 470 °C assigned to the reduction of surface Ce^{4+} species (15%) and another at 800 °C due to reduction of bulk species (8%). According to the H_2 uptake reported in Table 2, Co_3O_4 is completely reduced below 500 °C in the CoCe sample.

Fig. 4B shows the reduction profiles of the MnCo and MnCe bi-component samples. The MnCo sample shows two well-defined peaks at 313 and 487 °C. It has been reported that the manganese oxides (MnO_2, Mn_2O_3, and Mn_3O_4) could be reduced between 200 °C and 500 °C [26]. Therefore, the peak at 313 °C could be assigned to the reduction of Co^{3+} to Co^{2+} and a fraction of Mn_xO_y, while the other corresponds to the reduction of Co^{2+} to Co^0 and Mn^{4+}/Mn^{3+} to Mn^{2+}. According to the H_2 consumption of the first peak (Table 2) only the Co^{3+} species of the Co_3O_4 phase were reduced to Co^{2+} ($H_2/Co = 0.31$). From the total H_2 uptake, it is possible to conclude that the manganese Mn_xO_y and Co_3O_4 are partially reduced, with a molar ratio $H_2/(Co + Mn) = 0.8$.

On the other hand, the MnCe profile shows a narrow peak at 270 °C and another broad one at 360 °C that could be assigned to the reduction of Mn^{+4}/Mn^{+3} to Mn^{+2} species incorporated in the CeO_2 structure. Considering that the total of Mn^{+4} species are reduced to Mn^{+2} below 600 °C, the H_2 consumption in the 200–600 °C region (Table 2) suggests that 17% of Ce^{+4} surface species are reduced to Ce^{+3} while in the broad peak centered at 800 °C, associated with bulk ceria, the reduction of a remaining manganese oxide could be included.

The profiles of MnCoCe catalysts, with Mn/Co ratios of (1/8), (1/4) and (1/1), show three reduction zones at low (150–420 °C), intermediate (420–620 °C) and high (650–900 °C) temperatures (Fig. 5A). As shown by XRD, in these three samples, the Co species seems preferentially to form the Co_3O_4 spinel ($2\theta = 36.9°$) without distortion of the CeO_2 structure, which is reduced at low temperature. The reduction of manganese species should also be considered in this zone, because there are multiple overlapping peaks which change

Table 2 – TPR results.

Catalyst	Temperature range (°C)	Metal content (μmol)[a]			H_2 uptake (μmol)	$H_2/(Co + Mn + Ce)$
		Co	Mn	Ce		
CeO_2	250–550	–	–	581	44.98	0.077
	600–900				26.00	0.045
CoCe	100–600	154	–	560	256.2	0.358
	600–900				20.6	0.029
MnCo	150–370	1128.4	267.3	–	357.6	0.256
	370–640				754.1	0.540
MnCe	200–475	–	17.1	221.7	36.4	0.152
	650–900				23.1	0.097
MnCoCe(1/8)	100–430	173.1	20.0	189.8	176.2	0.460
	430–650				78.8	0.206
	650–900				43.4	0.113
MnCoCe(1/4)	100–375	188.2	47.7	178.4	145.8	0.352
	375–680				138.7	0.335
	680–900				30.1	0.073
MnCoCe(1/1)	100–400	176.7	180.4	155.7	194.7	0.380
	400–700				113.7	0.222
	700–900				24.9	0.048
MnCoCe(4/1)	100–450	192.3	803.1	65.0	457.2	0.431
	550–900				145.0	0.137

a The values (μmol of Co, Mn and Ce) were determined by ICP-AES in 100 mg of sample.

with the Mn concentration. Then, the cobalt species (Co_3O_4) and a fraction of Mn^{4+}/Mn^{+3} species incorporated to the ceria structure might be reduced below 420 °C. The reduction temperatures of Co_3O_4 in MnCoCe catalysts are lower than in the CoCe sample. In the intermediate region, as the manganese content increases, the temperature of maximum reduction rate also increases. This could correspond to the reduction of Mn^{3+}–Mn^{2+} species that belong to the mixed spinel $(Mn,Co)_3O_4$, as well as to the reduction of surface Ce^{4+} species. The other broad peak centered at 800 °C is a typical reduction peak of bulk CeO_2, and could also be associated with some difficult-to-reduce Mn^{n+} species.

Fig. 5B shows the reduction profile of MnCoCe(4/1) catalyst, where the amount of Ce is lower than in the other three catalysts. Three well-defined peaks can be observed, the first two at 289 °C and 374 °C corresponding to the reduction of Co_3O_4 and MnO_x, and the other at 690 °C with a shoulder around 800 °C that could correspond to the reduction of Mn^{3+}–Mn^{2+} species belonging to the mixed spinel $(Mn,Co)_3O_4$, as well as to reduction of Ce^{4+} bulk species.

Fig. 6A shows the Raman spectra of bi-component MnCe and CoCe catalysts as well as pure ceria. The CeO_2 spectrum shows a single peak at 464 cm^{-1}, attributed to the CeO_2 with fluorite structure. This band is due to the symmetric vibration of the oxygen atoms around the cerium ions [29,30]. In the MnCe spectrum, a weak signal at 594 cm^{-1} is also observed. As regards Mn–Ce compounds, Xu et al. [29] reported that Mn ions could be incorporated into the CeO_2 network increasing the structure defects with oxygen vacancies.

The bi-component CoCe spectrum shows the five Raman-activated modes of pure Co_3O_4. The band at 197 cm^{-1} is assigned to the tetrahedral sites (CoO_4) with F_{2g} symmetry. The Raman bands around 521 and 618 cm^{-1} also correspond to the F_{2g} symmetry modes, while 480 cm^{-1} is assigned to the E_g symmetry mode. The band around 689 cm^{-1} is attributed to the octahedral sites (CoO_6) with A1 symmetry [30,31]. A peak at 463 cm^{-1} is also observed and it corresponds to CeO_2.

Fig. 6B shows the spectra of bi-component MnCo and MnCoCe catalysts. The MnCoCe spectra show widening and a slight shift to a lower wavenumber in the peak associated with CeO_2, as the manganese incorporation increases. Hong et al.

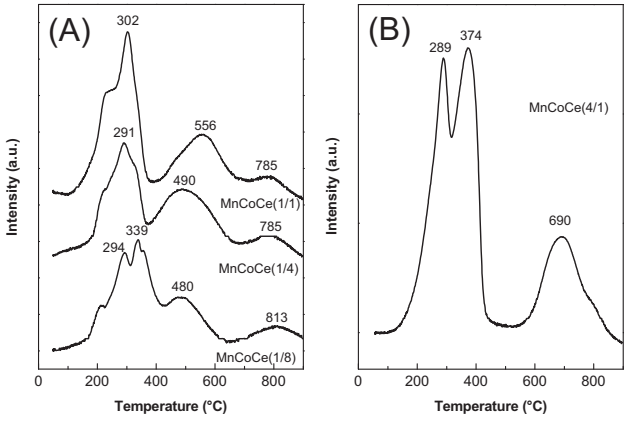

Fig. 5 – Temperature-programmed reduction of catalyst. (A) MnCoCe(1/8), MnCoCe(1/4), and MnCoCe(1/1). (B) MnCoCe(4/1).

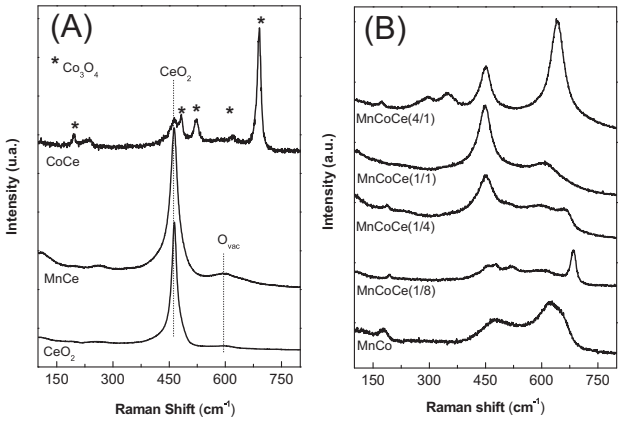

Fig. 6 – Raman spectra. (A) CeO_2, MnCe and CoCe. (B) MnCo, MnCoCe(1/8), MnCoCe(1/4), MnCoCe(1/1) and MnCoCe(4/1).

[32] found similar results in Mn–Ce samples and they attributed this effect to the introduction of Mn ions in the CeO_2 structure.

In the MnCoCe(1/8) spectrum, the peaks corresponding to the Co_3O_4 spinel can be clearly detected, while in MnCoCe(1/4), where the content of manganese is higher, these signals seem to be absent. Furthermore, an incipient peak at 666 cm^{-1} is observed. A possible substitution of Co ions by Mn ions might be occurring with the consequent formation of a Mn,Co mixed spinel. Nevertheless, in XRD analysis, the main peak corresponding to the Co_3O_4 spinel was present. Therefore, the co-existence of Co_3O_4 and $(Mn,Co)_3O_4$ phases could also be possible.

In MnCoCe(1/1), the peak at 450 cm^{-1} is considerably higher than other signals and it would be indicating a stronger Mn–Ce interaction. A broad and weak signal at around 609 cm^{-1}, which is less intense in MnCoCe(1/8) and MnCoCe(1/4) is also observed, and it might indicate the incipient formation of a Mn–Co compound.

Besides the peak assigned to CeO_2, the MnCoCe(4/1) spectrum shows a strong band at 641 cm^{-1} and other small signals at 174, 297 and 348 cm^{-1}. Several authors [33,34] have found the main signal of Mn_3O_4 around 641 cm^{-1}, as well as other signals around 350 and 293 cm^{-1} which might also be assigned to this phase.

In the 400–700 cm^{-1} range, the MnCo spectrum shows two broad signals and a small peak at 178 cm^{-1}. The signal between 550 and 700 cm^{-1} seems to be composed of two peaks, which might correspond to the main signals of Mn_3O_4 and Co_3O_4. In addition, between 400 and 500 cm^{-1} important peaks of these two species also appear. Again, the co-existence of Mn_3O_4 and Co_3O_4 could not be discarded.

In order to investigate the chemical state and surface concentration of species in the MnCoCe catalysts and bi-component samples, the photoelectron spectra of samples with different Mn/Co were analyzed. The binding energies (BE) of Co 2p, Mn 2p and O 1s core-level are shown in Table 3. The spectra of the Co $2p_{3/2}$ region of MnCoCe(1/8) sample presents the main peak at 780.0 ± 0.1 eV (FWHM = 3.0 eV) and a satellite peak centered at 785.3 eV (Fig. 7A). Also, the spin-orbit doublet Co $2p_{1/2}$–Co $2p_{3/2}$ was about 15.0 eV. Even though the BE

Table 3 – XPS data of Mn–Co–Ce compounds.

Catalyst	B.E. Co $2p_{3/2}$/eV		I_{sat}/I_{main}	B.E/eV				Molar surface ratio[c]		Molar bulk ratio[d]	
	Main peak	Satellite		Mn $2p_{3/2}$		O 1s		Co/Ce	Mn/Co	Co/Ce	Mn/Co
MnCoCe(1/8)	780.0 (3.0)[a]	785.3 (5.0)	0.22	641.2 (3.1) 644.9 (3.1)	77%	529.3 (2.2) 531.8 (2.9)	61%	0.17	0.26	0.91	0.12
MnCoCe(1/4)	780.0 (3.1)	785.0 (5.0)	0.25	641.3 (3.0) 644.7 (3.0)	80%	529.2 (2.0) 531.3 (2.8)	64%	0.19	0.39	1.06	0.25
MnCoCe(1/4)[b]	780.3 (3.3)	785.4 (5.5)	0.53	641.2 (3.1) 644.8 (3.1)	80%	529.2 (1.9) 531.4 (3.0)	53%	0.22	0.36	1.06	0.25
MnCoCe(1/1)	780.1 (3.0)	785.0 (5.2)	0.26	641.4 (2.9) 643.7 (3.1)	86%	529.3 (2.0) 531.2 (3.2)	54%	0.15	2.2	1.13	1.02
MnCoCe(4/1)	780.3 (2.8)	785.3 (5.1)	0.52	641.6 (3.0) 644.0 (3.0)	82%	529.6 (2.0) 531.9 (3.1)	55%	0.24	7.0	2.96	4.17
MnCe	–	–	–	641.4 (3.1) 644.9 (3.1)	71%	530.0 (2.0) 532.3 (2.7)	60%	–	–	–	–
MnCo	780.3 (3.7)	785.3 (5.3)	0.07	641.1 (3.1) 643.2 (3.1)	58%	530.0 (3.0) 533.7 (2.5)	90%	–	0.44	–	0.24
CoCe	780.0 (3.5)	785.3 (2.7)	0.11	–		529.5 (2.3) 531.9 (2.5)	73%	0.20	–	0.27	–
CeO_2	–	–	–	–		529.4 (2.0) 531.8 (3.0)	56%	–	–	–	–

a (Full width at half maximum).
b Sample used in the long term stability test for COPROX with CO_2.
c Molar surface ratio measured by XPS.
d Molar bulk ratio measured by ICP-AES.

values of Co^{3+} and Co^{2+} are relatively close, both oxidation states of cobalt can be distinguished by the presence of a distinct shake-up satellite structure in Co^{2+}, arising from the presence of unpaired electrons in the valence orbital. Co^{3+} is almost always in a low spin state and, therefore, there can be no energy transfer to an unpaired electron, meaning that a shake-up satellite structure is not observed [35,36].

The satellite intensity is relatively low, and the ratio to the main peak (I_{sat}/I_{main}) is lower than 0.26, which indicates that Co^{+3} is the predominant species on the surface [37]. The spinel Co_3O_4 contains two distinct types of cobalt ions; Co^{2+} and Co^{3+} in tetrahedral and octahedral coordination respectively, which are present in the surface of MnCoCe(1/8), (1/4) and (1/1), as previously shown by XRD. In addition, a $(Mn,Co)_3O_4$ phase had been previously proposed and it is possible that some Mn ions replace a Co^{3+} in Co_3O_4 spinel to form the mixed spinel phase.

However, in the catalysts with higher Mn content, MnCoCe(4/1), the Co $2p_{3/2}$ BE was 780.3 eV and the spin-orbit splitting Co $2p_{1/2}$–Co $2p_{3/2}$ was 15.2 eV. In addition, the ratio (I_{sat}/I_{main}) was 0.52, indicating a high concentration of Co^{2+} on the surface.

Fig. 7B shows Mn 2p spectra corresponding to the MnCoCe and MnCo samples. As it can be observed in the samples, Mn 2p spectra are composed of two main spin-orbit lines Mn $2p_{3/2}$ and Mn $2p_{1/2}$ around 641 eV and 652.5 eV, respectively. Both peaks show some asymmetry which suggests the presence of two components in each one (Table 3). The BE difference between Mn $2p_{1/2}$ and Mn $2p_{3/2}$ peaks was approximately 11.5 eV and the full width at half maximum in all samples was 3.1 ± 0.1 eV. The main component of Mn $2p_{3/2}$ peak, at 641.2 eV for MnCoCe(1/8), is associated with Mn^{+3} species, which is shifted to higher values as the Mn content increases. The other component close to 644.9 eV corresponds to Mn^{+4} species and these values slightly decrease as the manganese loading increases. However, the values reported in the literature for pure oxides are lower since for MnO, Mn_2O_3 and MnO_2 are approximately 641.2, 641.8 and 642.2 eV, respectively [38,39]. Likely, a strong interaction between the manganese with Co and Ce ions modifies these values. In this sense, for the Mn–Ce system, other authors reported BE values around 641 eV and 643 eV for Mn^{3+} and Mn^{4+}, respectively [40,41]. In addition, the spectral splitting of Mn 3s X-ray photoemission spectra was analyzed. Fig. 7C depicts the Mn 3s splitting of MnCoCe and MnCo samples. The largest splitting (about 6.2 eV) belongs to the MnCo sample. This value corresponds to MnO (Mn^{+2}) according to the XPS study by Galakhov et al. [42] on manganites. On the other hand, MnCoCe(4/1) and (1/1) showed Mn 3s splitting values of 5.1 and 5.2, respectively associated with the Mn valency of 3.0–3.3. In the other samples, MnCoCe(1/4) and (1/8), with lower Mn content no signal was detected in the Mn 3s spectra.

As can be observed in Fig. 7D, the asymmetrical O 1s signal can be fitted with two components in all samples. The dominant peak at 529.3–530.0 eV was assigned to surface lattice oxygen, and the other peak at higher BE was associated with surface oxygen ions with low coordination [43].

The Ce 3d region was also analyzed in the CoMnCe, CoCe, MnCe and CeO_2 samples. In calcined samples, only Ce^{4+} signals were observed. The spectra were fitted with six peaks whose binding-energy positions of MnCoCe and CoCe catalysts were very close to those found for the CeO_2 sample. As mentioned by several authors [44–46], the CeO_2 spectrum is composed by several peaks; for each component of spin–orbit split doublet (usually referred to as v and u and associated with Ce $3d_{5/2}$ and Ce $3d_{3/2}$, respectively) contains three peaks.

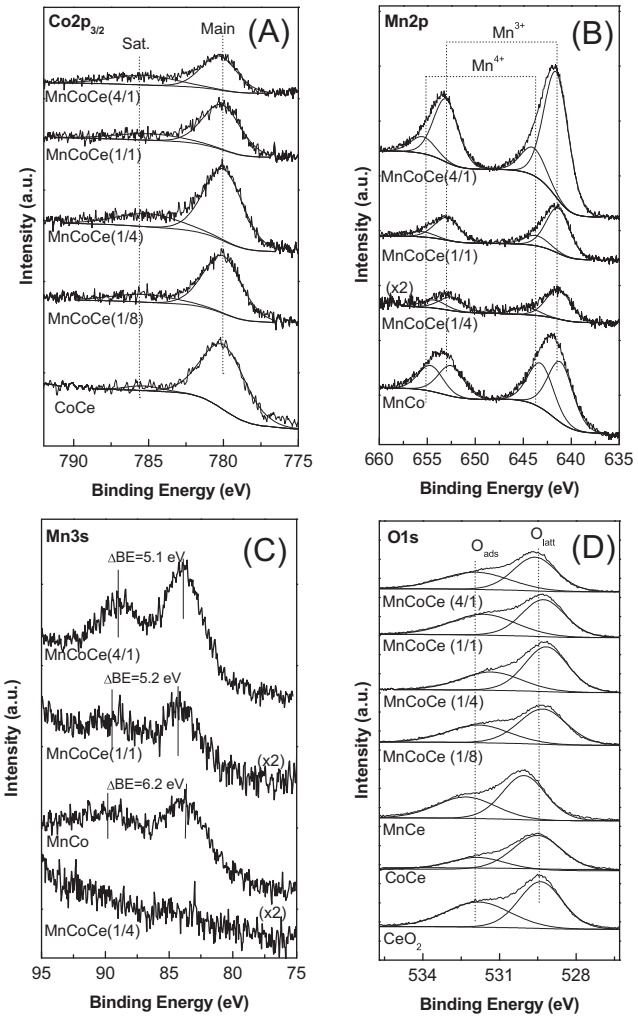

Fig. 7 – XPS spectra of Co $2p_{3/2}$ (A), Mn 2p (B), Mn 3s (C) and O 1s (D) for different samples.

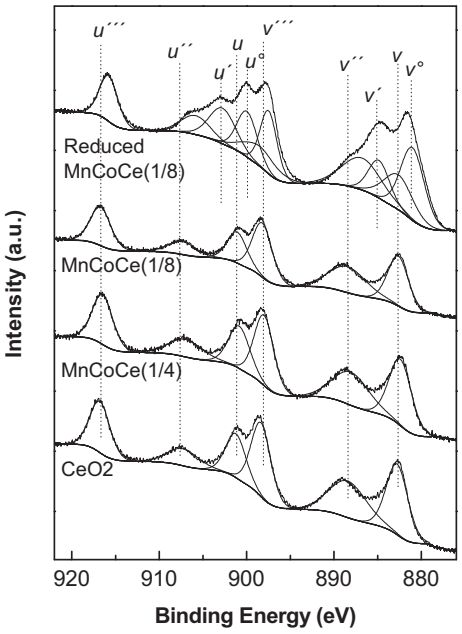

Fig. 8 – Ce3d XPS spectra of CeO_2, MnCoCe(1/4) and MnCoCe(1/8) calcined and reduced.

The lower binding energy peaks at 882.7, 888.4 and 898.3 eV, correspond to v, v'' and v''' peaks are characteristic of Ce $3d_{5/2}$, while other three peaks u, u'' and u''' located at 901.2, 907.3 and 916.8 eV, respectively were assigned to Ce $3d_{3/2}$. The spectra corresponding to calcined CeO_2, MnCoCe(1/4), MnCoCe(1/8) catalysts (Fig. 8) present the six mentioned peaks corresponding to Ce^{4+} of CeO_2. However, when sample MnCoCe(1/8) was reduced with a H_2/Ar flow at 300 °C in the pretreatment chamber of the spectrometer, there appeared four additional peaks associated with Ce^{3+} species. The Ce_2O_3 spectrum involves a spin-orbit split doublet with two peaks, $v°$ and v' at 881.0 and 884.2 eV belong to Ce $3d_{5/2}$, and $u°$ and u' at 898.5 and 902.8 eV correspond to Ce $3d_{3/2}$.

According to the surface ratios calculated from XPS data (Table 3), the concentration of Co in the surface of MnCoCe catalysts is lower than the bulk composition, while an enrichment surface of manganese is observed.

Finally, the MnCoCe(1/4) catalyst, previously used in reaction with CO_2 addition during 75 h was analyzed by the XPS technique. No significant change in the binding energies of the constituent elements was observed. In the Co $2p_{3/2}$ region, an increase of 0.25–0.53 in the I_{sat}/I_{main} ratio was calculated and this indicates a higher Co^{2+} proportion due to the reductive atmosphere of the reaction mixture. On the other hand, the formation of carbonate species as a consequence of the reaction was not observed on the catalyst surface.

4. Conclusions

Catalysts composed of Mn–Co–Ce mixed oxides are active, selective and stable for the COPROX reaction. Among the formulations we studied, the one containing a Mn/Co ratio equal to 1/4 showed to be the most active. The activity trend we observed for different Mn/Co ratios was 1/4 > 1/1 > 1/8–0/1–4/1 ≫ 1/0 (CO conversions measured at 125 °C, and oxygen selectivity higher than 90%). When Mn was added in small amounts to the Co–Ce solid, the surface area increased and for a higher Mn loading it decreased. Thus, two important factors could be related to the increase of CO conversion when small amounts of Mn were added: the increase on surface area and the improvement in redox properties of Co. In general, these results are in line with those reported by other authors for similar catalysts.

In order to gain insight into the physical chemistry properties of the system under study, we carried out a careful spectroscopic characterization. XPS results show that in all cases the catalytic surface is enriched in Mn, while the opposite occurs in Co. Thus, the low activity for catalysts with a high Mn loading could be related to the lack of accessibility of reactant molecules to Co active sites (note that for the sample with a Mn/Co ratio of 4/1 the surface Mn:Co ratio is 7/1). It is also shown that, after 75 h of time-on-stream with CO_2 included in the feed, no carbonate formation was detected for the more active sample, and the surface atomic ratios remained constant, results that are in line with the high

catalytic stability of the sample. The only effect we observed after reaction was a strong increase of the Co^{2+}/Co^{3+} surface ratio. This surface reduction probably took place at the beginning of the reaction due to the strong reductive environment; however, metallic Co was not detected.

In all the Co–Mn–Ce samples, we observed the formation of partially developed $(Mn,Co)_3O_4$ mixed spinels. The presence of these species, that are reduced during TPR experiments at an intermediate temperature range (300–600 °C), was also inferred from XRD and LRS results.

Acknowledgments

The authors acknowledge the financial support received from UNL and CONICET. They are grateful to ANPCyT for the purchase of the SPECS multitechnique analysis instrument (PME 8-2003), the TPD/TPR/TPO system (PME-2007-071) and the UV–Vis spectrometer (PME 311-2006). Thanks are given to Fernanda Mori for the XPS measurements and to Elsa Grimaldi for the English language editing.

REFERENCES

[1] Bion N, Epron F, Moreno M, Mariño F, Duprez D. Preferential oxidation of carbon monoxide in the presence of hydrogen (PROX) over noble metals and transition metal oxides: advantages and drawbacks. Top Catal 2008;51:76–88.
[2] Li D, Liu X, Zhang Q, Wang Y, Wan H. Cobalt and copper composite oxides as efficient catalysts for preferential oxidation of CO in H_2-rich stream. Catal Lett 2009;127:377–85.
[3] Mariño F, Descorme C, Duprez D. Supported base metal catalysts for the preferential oxidation of carbon monoxide in the presence of excess hydrogen (PROX). Appl Catal B 2005;58:175–83.
[4] Ko EY, Park ED, Seo KW, Lee HC, Lee D, Kim S. A comparative study of catalysts for the preferential CO oxidation in excess hydrogen. Catal Today 2006;116:377–83.
[5] Korotkikh O, Farrauto R. Selective catalytic oxidation of CO in H_2: fuel cell applications. Catal Today 2000;62:249–54.
[6] Luengnaruemitchai A, Nimsuk M, Naknam P, Wongkasemjit S, Osuwan S. A comparative study of synthesized and commercial A-type zeolite-supported Pt catalysts for selective CO oxidation in H_2-rich stream. Int J Hydrogen Energy 2008;33:206–13.
[7] Wang C, Li B, Lin H, Yuan Y. Carbon nanotube-supported Pt–Co bimetallic catalysts for preferential oxidation of CO in a H_2-rich stream with CO_2 and H_2O vapor. J Power Sources 2012;202:200–8.
[8] Potemkin DI, Filatov EY, Zadesenets AV, Snytnikov PV, Shubin YV, Sobyanin VA. Preferential CO oxidation over bimetallic Pt–Co catalysts prepared via double complex salt decomposition. Chem Eng J 2012;207–208:683–9.
[9] Ayastuy JL, Gil-Rodríguez A, González-Marcos MP, Gutiérrez-Ortiz MA. Effect of process variables on Pt/CeO_2 catalyst behavior for the PROX reaction. Int J Hydrogen Energy 2006;31:2231–42.
[10] Galletti C, Fiorot S, Specchia S, Saracco G, Specchia V. Catalytic performance of $Au–TiO_2$ catalysts prepared by deposition-precipitation for CO preferential oxidation in H_2-rich gases. Chem Eng J 2007;134:45–50.
[11] Quinet E, Morfin F, Diehl F, Avenier P, Caps V, Rousset JL. Hydrogen effect on the preferential oxidation of carbon monoxide over alumina-supported gold nanoparticles. App Catal B 2008;80:195–201.
[12] Avgouropoulos G, Manzoli M, Boccuzzi F, Tabakova T, Papavasiliou J, Ioannides T, et al. Catalytic performance and characterization of Au/doped-ceria catalysts for the preferential CO oxidation reaction. J Catal 2008;256:237–47.
[13] Mariño F, Baronetti G, Laborde M, Bion N, Le Valant A, Epron F, et al. Optimized $CuO–CeO_2$ catalysts for COPROX reaction. Int J Hydrogen Energy 2008;33:1345–53.
[14] Martínez-Arias A, Gamarra D, Fernández-García M, Wang XQ, Hanson JC, Rodriguez JA. Comparative study on redox properties of nanosized CeO_2 and CuO/CeO_2 under CO/O_2. J Catal 2006;240:1–7.
[15] Zhang F, Chen C, Xiao W, Xu L, Zhang N. CuO/CeO_2 catalysts with well-dispersed active sites prepared from $Cu_3(BTC)_2$ metal-organic framework precursor for preferential CO oxidation. Catal Commun 2012;26:25–9.
[16] Marbán G, Fuertes AB. Highly active and selective CuO_x/CeO_2 catalyst prepared by a single-step citrate method for preferential oxidation of carbon monoxide. Appl Catal B 2005;57:43–53.
[17] Gómez LE, Tiscornia IS, Boix AV, Miró EE. CO preferential oxidation on cordierite monoliths coated with Co/CeO_2 catalysts Int. J Hydrogen Energy 2012;37:14812–9.
[18] Chen YZ, Liaw BJ, Wang JM, Huang CT. Selective removal of CO from hydrogen-rich stream over $CuO/Ce_xSn_{1-x}O_2–Al_2O_3$ catalysts. Int J Hydrogen Energy 2008;33:2389–99.
[19] Wu Z, Zhu H, Qin Z, Wang H, Huang L, Wang J. Preferential oxidation of CO in H_2-rich stream over $CuO/Ce_{1-x}Ti_xO_2$ catalysts. Appl Catal B 2010;98:204–12.
[20] Zhao Z, Lin X, Jin R, Dai Y, Wang G. High catalytic activity in CO PROX reaction of low cobalt-oxide loading catalysts supported on nano-particulate $CeO_2–ZrO_2$ oxides. Catal Commun 2011;12:1448–51.
[21] Zhao Z, Lin X, Jin R, Wang G, Muhammad T. MO_x (M = Mn, Fe, Ni or Cr) improved supported Co_3O_4 catalysts on ceria–zirconia nanoparticulate for CO preferential oxidation in H_2-rich gases. Appl Catal B 2012;115–116:53–62.
[22] Zhao Z, Jin R, Bao T, Yang H, Lin X, Wang G. Mesoporous $Ce_xMn_{1-x}O_2$ composites as novel alternative carriers of supported Co_3O_4 catalysts for CO preferential oxidation in H_2 stream. Int J Hydrogen Energy 2012;37:4774–86.
[23] Guo Q, Liu Y. MnO_x modified $Co_3O_4–CeO_2$ catalysts for the preferential oxidation of CO in H_2-rich gases. Appl Catal B 2008;82:19–26.
[24] Guo Q, Chen S, Liu Y, Wang Y. Stability of Co–Ce–Mn mixed-oxide catalysts for CO preferential oxidation in H_2-rich gases. Chem Eng J 2010;165:846–50.
[25] Zhang Q, Liu X, Fan W, Wang Y. Manganese-promoted cobalt oxide as efficient and stable non-noble metal catalyst for preferential oxidation of CO in H_2 stream. Appl Catal B 2011;102:207–14.
[26] Picasso G, Gutiérrez M, Pina MP, Herguido J. Preparation and characterization of Ce–Zr and Ce–Mn based oxides for *n*-hexane combustion: application to catalytic membrane reactors. Chem Eng J 2007;126:119–30.
[27] Morales F, Grandjean D, Mens A, De Groot FMF, Weckhuysen BM. X-ray absorption spectroscopy of Mn/Co/TiO_2 Fischer-Tropsch catalysts: relationships between preparation method, molecular structure, and catalyst performance. J Phys Chem B 2006;110:8626–39.
[28] Gawade P, Bayram B, Alexander AMC, Ozkan US. Preferential oxidation of CO (PROX) over CoO_x/CeO_2 in hydrogen-rich streams: effect of cobalt loading. Appl Catal B 2012;128:21–30.

[29] Xu J, Li P, Song X, He C, Yu J, Han YF. Operando Raman Spectroscopy for determining the active phase in one-dimensional $Mn_{1-x}Ce_xO_{2\pm y}$. Nanorod catalysts during methane combustion. J Phys Chem Lett 2010;1:1648–54.
[30] Woods MP, Gawade P, Tan B, Ozkan US. Preferential oxidation of carbon monoxide on Co/CeO_2 nanoparticles. Appl Catal B 2010;97:28–35.
[31] Alvarez A, Ivanova S, Centeno MA, Odriozola JA. Sub-ambient CO oxidation over mesoporous Co_3O_4: effect of morphology on its reduction behavior and catalytic performance. Appl Catal A 2012;431–432:9–17.
[32] Hong WJ, Iwamoto S, Hosokawa S, Wada K, Kanai H, Inoue M. Effect of Mn content on physical properties of CeO_x–MnO_y support and BaO–CeO_x–MnO_y catalysts for direct NO decomposition. J Catal 2011;277:208–16.
[33] Han YF, Chen F, Zhong Z, Ramesh K, Chen L, Widjaja E. Controlled synthesis, characterization, and catalytic properties of Mn_2O_3 and Mn_3O_4 nanoparticles supported on mesoporous silica SBA-15. J Phys Chem B 2006;110:24450–6.
[34] Gao T, Fjellvåg H, Norby P. A comparison study on Raman scattering properties of α- and β-MnO_2. Anal Chim Acta 2009;648:235–9.
[35] Hagelin-Weaver HAE, Hoflund GB, Minahan DM, Salaita GN. Electron energy loss spectroscopic investigation of Co metal, CoO, and Co_3O_4 before and after Ar^+ bombardment. Appl Surf Sci 2004;235:420–48.
[36] Liotta LF, Di Carlo G, Pantaleo G, Venezia AM, Deganello G. Co_3O_4/CeO_2 composite oxides for methane emissions abatement: relationship between Co_3O_4–CeO_2 interaction and catalytic activity. Appl Catal B 2006;66:217–27.
[37] Pietrogiacomi D, Tuti S, Campa MC, Indovina V. Cobalt supported on ZrO_2: catalysts characterization and their activity for the reduction of NO with C_3H_6 in the presence of excess O_2. Appl Catal B 2000;28:43–54.
[38] Liang S, Teng F, Bulgan G, Zong R, Zhu Y. Effect of phase structure of MnO_2 nanorod catalyst on the activity for CO oxidation. J Phys Chem C 2008;112:5307–15.
[39] Ramesh K, Chen L, Chen F, Liu Y, Wang Z, Han YF. Re-investigating the CO oxidation mechanism over unsupported MnO, Mn_2O_3 and MnO_2 catalysts. Catal Today 2008;131:477–82.
[40] Qi G, Yang RT. Characterization and FTIR studies of MnO_x–CeO_2. Catalyst for low-temperature selective catalytic reduction of NO with NH_3. J Phys Chem B 2004;108:15738–47.
[41] Zou ZQ, Meng M, Zha YQ. Surfactant-assisted synthesis, characterizations, and catalytic oxidation mechanisms of the mesoporous MnO_x–CeO_2 and Pd/MnO_x–CeO_2 catalysts used for CO and C_3H_8 oxidation. J Phys Chem C 2010;114:468–77.
[42] Galakhov VR, Demeter M, Bartkowski S, Neuman M, Ovechkina NA, Kurmaev EZ, et al. Mn 3s exchange splitting in mixed-valence manganites. Phys Rev B: Condens Matter Mater Phys 2002;65:113102-1–113102-4.
[43] Wang F, Dai H, Deng J, Bai G, Ji K, Liu Y. Manganese oxides with rod-, wire-, tube-, and flower-like morphologies: highly effective catalysts for the removal of toluene. Environ Sci Technol 2012;46:4034–41.
[44] Le Normand F, Hilaire L, Kili K, Krill G, Mairet G. Oxidation state of cerium in cerium-based catalysts investigated by spectroscopic probes. J Phys Chem 1988;92:2561–8.
[45] Larachi F, Pierre J, Adnot A, Bernis A. Ce 3d XPS study of composite $Ce_xMn_{1-x}O_{2-y}$ wet oxidation catalysts. Appl Surf Sci 2002;195:236–50.
[46] Swiatowska J, Lair V, Pereira-Nabais C, Cote G, Marcus P, Chagnes AXPS. XRD and SEM characterization of a thin ceria layer deposited onto graphite electrode for application in lithium-ion batteries. Appl Surf Sci 2011;257:9110–9.